

1 **Simulating the transportation and dispersal of volcanic**
2 **ash cloud with initial condition created by 3D plume**
3 **model**

4 **Key Points:**

- 5 • The traditional way of generating initial condition for VATD simulation is based
6 on empirical expression for the height-MER relation. Creating initial condition
7 based on 3D plume model eliminates assumptions regarding ash particle distri-
8 bution of initial ash cloud and improves prediction capability.
9 • Initial particle distribution in vertical direction has more significant impact on trans-
10 portation of ash clouds than horizontal distribution.
11 • Ash particles are concentrated along intrusion height of umbrella cloud that is much
12 lower than the plume top, which is just momentum overshoot.

13 **Abstract**

14 VATD (volcanic ash transportation and dispersion) models require initial conditions, which
 15 describe the initial locus of ash that is then transported. Most VATD models use a line
 16 source of some prescribed shape calibrated against an empirical expression for the height-
 17 MER relation. Such empirical vertical ash distributions may not be good representations
 18 of actual vertical ash distributions, which usually vary from case to case and have com-
 19 plex dependencies on eruption source parameters and atmospherics conditions. 3D (three-
 20 dimensional) plume models provide an alternative way to create initial ash cloud with-
 21 out any assumption regarding plume geometry. By eliminating assumed behavior asso-
 22 ciated with the semiempirical plume geometry, the predict capacity of VATD simulation
 23 would be improved. However, no VATD simulation adopts initial condition created from
 24 3D plume simulation yet. We explore this option for the first time in this paper. A vol-
 25 canic plume model based on Lagrangian method is adopted to cooperate with another
 26 Lagrangian VATD model to demonstrate implementation details. The importance of ini-
 27 tial condition is shown in sensitivity analyses which prove that volcanic ash transpor-
 28 tation simulation is much more sensitive to initial condition than all other input param-
 29 eters. Further investigation reveals that initial particle distribution in vertical direction
 30 has more significant impact on transportation of ash clouds than horizontal distribution.
 31 Comparison also indicates that ash particles are concentrated along intrusion height of
 32 umbrella cloud that is much lower than the plume top, which is just momentum over-
 33 shoot.

34 **1 Introduction**

35 **1.1 Volcanic Ash Transportation Forecast**

36 The fine-grained fraction of tephra (volcanic ash) can be widely dispersed and can
 37 lead to a degradation of air quality and pose threats to aviation. Identification of vol-
 38 canic ash helps schedule the flights accordingly to avoid flying through area where ash
 39 presents. Numerical estimation of ash distribution using known wind fields is necessary
 40 if we are to accurately predict ash cloud evolution. Numerous VATD (volcanic ash trans-
 41 portation and dispersion) models have been developed by both civil and military avi-
 42 ation or meteorological agencies to provide forecasts of ash cloud motion (Witham et al.,
 43 2007). New techniques have been integrating with VATD to satisfy increasing demands
 44 for model accuracy and forecast reliability. This paper explores an alternative way for
 45 creating initial condition for VATD simulations, which promises to improve predict ca-
 46 pability and accuracy.

47 As has been reported (e.g. Fero et al., 2009) and will be confirmed in this paper,
 48 initial condition has significant effects on simulation of volcanic ash transportation. Tra-
 49 ditional VATD simulation usually requires key global descriptors of the volcanic plumes.
 50 It is a common practice to pick up the “best match” key global descriptors by param-
 51 eter calibration (e.g. Fero et al., 2008, 2009; Zidikheri et al., 2017). Often, 1D plume mod-
 52 els also serve as an alternative option to provide the key global descriptors. For exam-
 53 ple, Bursik et al. (2012) and Stefanescu et al. (2014) use bent (Bursik, 2001) to gener-
 54 ate global descriptors. No matter how are these global descriptors obtained, they are used
 55 to define the initial condition for VATDs in forms of line source term which furnishes VATD
 56 with a spatio-temporal distribution of particles/mass along the eruption column. Ver-
 57 tical mass/particle distribution of line source term is calibrated against an empirical ex-
 58 pression for the height-MER relation. The empirical expressions are written as functions
 59 of several parameters including key global descriptors. Sometimes, an extra step is adopted
 60 to spread ash particles of line source horizontally resulting in an initial ash cloud in 3D
 61 space. The horizontal spreading also depends on empirical expression. For example, PUFF
 62 spreads particle of line source uniformly in the horizontal direction within a given ra-
 63 dius. That is to say, both vertical distribution and horizontal distribution, if applicable,

64 are based on empirical expressions. Considering the complexities of volcano eruption,
 65 the actual ash distribution in initial ash clouds should vary from case to case. It is dif-
 66 ficult to have one general expression that suitable for all cases. So it is necessary to in-
 67 vestigate alternatives ways for creating initial ash clouds without assumptions on plume
 68 geometry. This is one major motivation of this paper.

69 1.2 Numerical Tools

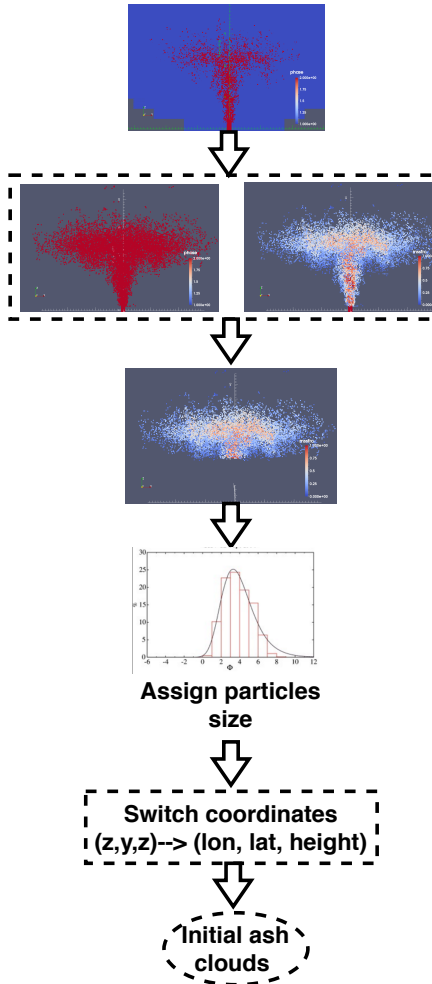
70 VATD models can be categorized into particle tracking type and advection-diffusion
 71 type. Among several available particle tracking models (e.g. Walko et al., 1995; Searcy
 72 et al., 1998; D'amours, 1998; Draxler & Hess, 1998) and advection-diffusion models (e.g.
 73 Bonadonna & Houghton, 2005; Folch et al., 2009; Schwaiger et al., 2012), we adopt a par-
 74 ticle tracking model, PUFF (Tanaka, 1991; Searcy et al., 1998), as the VATD model. PUFF
 75 can take 3D ash clouds as initial condition, which makes it technically easier to coop-
 76 erate with 3D plume models. PUFF initializes a discrete number of tracers that repre-
 77 sent a sample of the eruption cloud, and calculates transport, turbulent dispersion, and
 78 fallout for each representative tracer. While a cylinder emanating from the summit to
 79 a specified maximum height is the standard approach to crudely model the geometry of
 80 a typical ash column. It minimally requires horizontal wind field data. The “restart fea-
 81 ture” of PUFF makes it technically feasible to handle the difference between plume sim-
 82 ulation and VATD simulation in terms of time scale and length scales.

83 Besides parameters calibration, 1D (one dimensional) plume models are also adopted
 84 to get global descriptors of volcanic plume. 1D plume models (e.g. Woods, 1988; Bur-
 85 sik, 2001; Mastin, 2007; de'Michieli Vitturi et al., 2015; Folch et al., 2016; Pouget et al.,
 86 2016) usually simplify the scenario and account for mass, momentum and energy con-
 87 servation in 1D. Due to the simplification in 1D plume models, the entrainment of air
 88 is evaluated based on two coefficients: entrainment coefficient due to turbulence in the
 89 rising buoyant jet and the crosswind field. Different 1D models adopt different entrain-
 90 ment coefficients based on specific formulation or calibration against well-documented
 91 case studies. The feedback from plume to atmosphere is usually ignored in 1D models.
 92 While these 1D models generated well-matched results with 3D models for weak plumes,
 93 much greater variability is observed for strong plume scenarios, especially in terms of lo-
 94 cal variables (Costa et al., 2016). On the other hand, first principle based, entrainment
 95 coefficients free, 3D numerical models for volcanic plume (Oberhuber et al., 1998; Neri
 96 et al., 2003; Y. J. Suzuki et al., 2005; Cerminara, Esposti Ongaro, & Berselli, 2016; Cao
 97 et al., 2018) not only provides more accuracy prediction but also naturally create a 3D
 98 ash cloud, which can perfectly serves as initial condition for VATDs. However, to the best
 99 of author's knowledge, there is no VATD simulation taking such 3D ash clouds as ini-
 100 tial condition yet. In this paper, we will carry out VATD simulation with initial ash cloud
 101 based on 3D plume simulation for the first time. Among these 3D plume models, we choose
 102 Plume-SPH (Cao et al., 2018) due to its easy availability to our group.

103 Theoretically, implementation techniques described in this paper can be applied
 104 for any combination of VATD model and 3D plume model even though our investiga-
 105 tion is based on a specific VATD model and plume model.

106 1.3 Pinatubo Eruption

107 The 1991 eruption of Mountain Pinatubo is used as case study in this chapter. The
 108 Mountain Pinatubo erupted between June 12 and 16, 1991, after weeks of precursory ac-
 109 tivity. The climactic phase starts at June 15th 0441 UTC and ends around 1341 UTC
 110 (R. Holasek et al., 1996). This climactic phase generated voluminous pyroclastic flows
 111 and sent Plinian and co-ignimbrite ash and gas columns to great altitudes (Scott et al.,
 112 1996). The evolution of the Pinatubo ash and SO_2 clouds was tracked using the visual
 113 spectrum (R. Holasek et al., 1996), the ultraviolet spectrum with a total ozone mapping



122 **Figure 1.** The work flow to create initial condition for PUFF based on raw output of Plume-
 123 SPH. Figure on the top shows raw output of Plume-SPH, where, blue particles are for phase 1
 124 (ambient air), red particles are for phase 2 (erupted material). Pictures on the second row are
 125 plume after removing SPH particles of phase 1. The left picture is colored according to mass
 126 fraction of erupted material. The figure on the third row is volcanic plume after cutting off lower
 127 portion.

114 spectrometer (TOMS) (Guo, Bluth, et al., 2004), and the infrared spectrum with a va-
 115 riety of sensors, including advanced very high-resolution radiometer (AVHRR) (Guo, Rose,
 116 et al., 2004). There are also sufficient observational data to estimate the eruption con-
 117 dition for climactic phase of Pinatubo eruption (Y. Suzuki & Koyaguchi, 2009). The avail-
 118 ability of calibrated eruption condition and extensive observational data regarding ash
 119 clouds transportation makes the Pinatubo eruption an ideal case for our research.

120 2 Setting up Simulations

121 2.1 Creating of Initial Ash Cloud

128 The steps to create initial ash cloud based on raw output of Plume-SPH are shown
 129 in Fig. 1. The method proposed in this paper generates initial ash cloud directly from
 130 output of 3D plume model casting aside assumptions regarding plume shape. We take

131 Plume-SPH as an example. In case of other 3D plume models, the steps are similar. Plume-
 132 SPH is a two phases model based on a Lagrangian method, smoothed particle hydrody-
 133 namics (SPH), in which, the computational domain is discretized by SPH particles. The
 134 current version, Plume-SPH 1.0 (Cao et al., 2018), uses two types of SPH particles, par-
 135 ticle of phase 1 to represent ambient air and particles of phase 2 to represent erupted
 136 material. Initial ash cloud is created from SPH particle of phase 2 in this paper. After
 137 reaching to the maximum height and starting spreading horizontally, particles of phase
 138 2 forms an initial ash cloud, see, Fig. 2. 3D plume simulation is considered being com-
 139 pleted at this point. The lower part of the plume keeps moving vertically upwards and
 140 hence is involved only minimally in horizontal ash transport. Thereby, we cut off the lower
 141 part of the plume according to an elevation threshold. Considering SPH particles are es-
 142 sentially discretization points and have no size, we need to assign grain size to each par-
 143 ticle according to given distribution, mean and standard deviation of grain size (Paladio-
 144 Melosantos et al., 1996). As a consequence, the discretization points (has no size) are
 145 switch to Lagrangian tracers with sizes. The coordinates of these tracers, which are in
 146 the local Cartesian coordinate system of Plume-SPH, need to convert into PUFF's global
 147 coordinate system, which is written in terms of (*longitude, latitude, height*). PUFF then
 148 takes the initial ash clouds consisting of batch of Lagrangian tracers and propagates from
 149 time t to time $t + \Delta t$ via an advection/diffusion equation (Searcy et al., 1998).

$$150 \quad \mathbf{R}_i(t + \Delta t) = \mathbf{R}_i(t) + \mathbf{W}(t)\Delta t + \mathbf{Z}(t)\Delta t + \mathbf{S}_i(t)\Delta t \quad (1)$$

151 Here, $\mathbf{R}_i(t)$ is the position vector of i th Lagrangian tracer at time t , \mathbf{W} accounts for wind
 152 advection, \mathbf{Z} accounts for turbulent dispersion and \mathbf{S} is the terminal gravitational fall-
 153 out velocity, which depends on tracer's size.

154 To summarize, it takes four steps to create initial ash cloud from raw output of Plume-
 155 SPH:

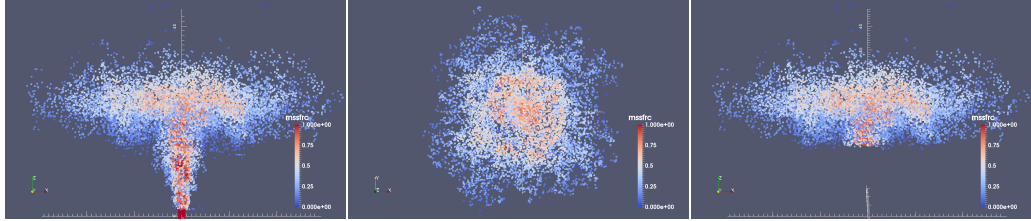
- 156 1. filtering by SPH particle type to select SPH particles that represent erupted ma-
 157 terial (phase 2)
- 158 2. filtering by an elevation threshold to cut off the plume, only leaving the upper part
- 159 3. switching discretization points to Lagrangian tracers by assigning grain size to each
 160 particle
- 161 4. converting coordinates of Lagrangian tracers into VATDs' coordinate system

162 The volcanic plume and initial ash clouds used in the case study are shown in Fig. 2.
 163 It is necessary to point out that since both Plume-SPH and PUFF are based on Lagrangian
 164 method, no extra step for conversion between Lagrangian particles and Eulerian grids.

172 Table 1 compares three different methods for creating initial conditions for VATD
 173 simulation: 1) creating initial condition based on parameter calibration without any plume
 174 model (method 1), 2) creating initial condition based on output of 1D plume model (method
 175 2), 3) extracting initial ash cloud from 3D plume simulation (method 3). The first method
 176 determines all global descriptors of volcanic plume based on calibration. Then create ini-
 177 tial line source or ash cloud according to semiempirical plume shape expression. Both
 178 other two methods depend on plume models. However 3D plume models can generate
 179 initial ash cloud in 3D space while 1D plume models only obtain global descriptors of
 180 plume so still need semiempirical expression to create 3D initial ash cloud. In addition,
 181 the number of Lagrangian tracers is a free parameter when using semiempirical plume
 182 shape expressions while it purely depends on simulation when creating initial condition
 183 from 3D plume simulation results.

186 2.2 Restart PUFF

187 The plume development and ash transportation are of different time scale and length
 188 scale. Spatial and temporal resolution of plume simulation is much finer than that of ash



165 **Figure 2.** All particles in the pictures are of type phase 2 (phase 1 has been removed in step
 166 1) at 600s after eruption, at which time, the plume has already reached the maximum height
 167 and started spreading radially. Pictures from left to right are: front view of the whole plume,
 168 top view of the plume and front view of the initial ash cloud, which is essentially portion of the
 169 whole plume with elevation higher than a given threshold (in this picture is 15000m). Particles
 170 are colored according to mass fraction of erupted material. Red represents high mass fraction
 171 while blue represents low mass fraction.

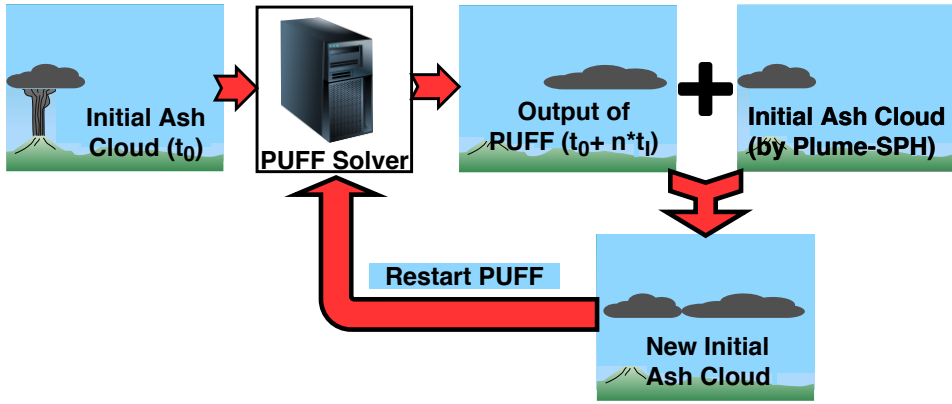
184 **Table 1.** Three different methods for creating initial conditions (initial ash clouds) for PUFF
 185 simulation

	No model	1D model	3D model
Maximum height	Calibration	Semiempirical	1st principle
Average height	Calibration	Conservation laws (1D)	1st principle
Vertical spread	Calibration	Semiempirical	1st principle
Column radius	Calibration	Conservation laws (1D)	1st principle
Plume shape	Semiempirical	Semiempirical	1st principle
Tracers number	Free parameter	Free Parameter	Based on simulation

189 transportation. The computational domain of VATD simulation is much larger than that
 190 of plume simulation. It takes around tens of minutes (600s in this case) for Pinatubo plume
 191 to reach a steady height. However the duration of eruption persists for a few hours (9
 192 hours for the climactic phase of Pinatubo eruption). It is computationally too expen-
 193 sive to do 3D plume simulation up to several hours. In order to handle the difference in
 194 time scale, we mimic successive eruption with intermittent pulsing releasing of ash par-
 195 ticles. Particularly, we restart PUFF at an interval of 600s, which is physical time of plume
 196 simulation. At every restart, we integrate the output of last PUFF simulation and the
 197 ash cloud obtained from output of Plume-SPH into a new ash cloud. This new ash cloud
 198 serves as a new initial condition when restart PUFF simulation. The interval of the puls-
 199 ing release equals to the simulation time of plume model, that is 600s in our case study.
 200 A sketch demonstrating the overall restart process is in Fig. (3). The total number of
 201 Lagrangian tracers used in PUFF equals to summation of numbers of particles in all re-
 202 leases. So the total number of tracers is not a parameter selected by user any more. Fero
 203 et al. (2008) proposed using more realistic time-dependent plume heights. We do not adopt
 204 that strategy here due to lack of well-estimated time-dependent eruption conditions, al-
 205 though the idea is straightforward to consider.

208 2.3 Sensitivity Analysis of Other Parameters

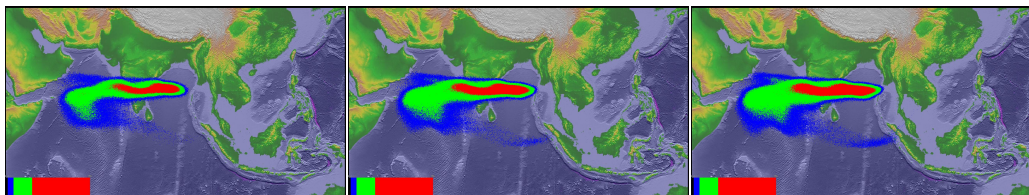
209 Besides the initial ash cloud, other input parameters for PUFF simulation are: hor-
 210 izontal diffusivity, vertical diffusivity, mean grain size, grain size standard deviation and
 211 total number of tracers. We present in this subsection systematic sensitivity studies on
 212 these parameters. We also investigate the influence of eruption duration. The sensitiv-



206 **Figure 3.** Mimic successive eruption with intermittent pulsing releasing of ash particles. t_I is
207 the period of pulsing release. t_I equals to physical time of 3D plume simulation.

213 ity analyses will serve as basis for identifying possible sources of disparities between sim-
214 ulation and observation.

215 The sensitivity analyses illustrate that adjustment of other input parameters pro-
216 duces negligible visual differences in VATD simulation results. Using different vertical
217 diffusivities in range of $[100, 100000] m^2 s^{-1}$ and different horizontal diffusivities in range
218 of $[1, 20] m^2 s^{-1}$ produces visually negligible differences. The eruption duration should
219 depend on the actual eruption duration (or the duration of climactic phase) of a specific
220 eruption. We conducted several simulations with eruption duration varying in range of
221 $[5, 11] hours$ with slight different starting time of climactic phase. Table 2 lists all these
222 simulations. However, only tiny visible differences are observed among the simulated ash
223 transportation. The mean of grain size also has visually ignorable effects on long-term
224 ash transportation according to our sensitivity tests varying the log mean (base 10) grain
225 radius in a range of $[-7.3, -3.5] m$. The standard deviation, when varying in range of $[0.1, 10]$,
226 generate ignorable difference on long-term ash transportation as well. Similar conclu-
227 sion on parameter sensitivity is reported by Fero et al. (e.g. 2008); Daniele et al. (e.g.
228 2009). Among these parameters, the eruption duration and beginning time shows, even
229 though tiny, the most obvious influence on simulated ash distribution. In order to show
230 such differences in an intuitive way, Fig. 2 shows simulated ash distribution correspond-
231 ing to 4.9 hours duration, 9 hours duration and 11 hours duration respectively. After 72
232 hours, relative to the simulation starting time, these three cases generate generally sim-
233 ilar results, with high concentration ash covers almost the same region. The difference
234 of lower concentration distribution is relatively more obvious. Ash cloud covers broad-
235 est area when eruption duration is 11.1 hours. To summarize, all these parameters have
236 either tiny or ignorable affects on long-term ash distribution simulation.

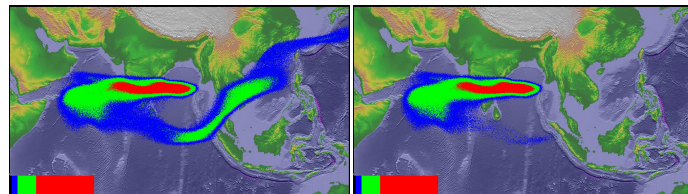


240 **Figure 4.** Simulated ash cloud distribution corresponding to eruption duration of 4.9 hours, 9
241 hours and 11.1 hours (from left to right) respectively. Starting and ending time for each case is in
242 Table 1. The contours are for ash distribution at 72 hours after eruption.

237 **Table 2.** The starting and ending time (UT) for simulating the climactic phase of Pinatubo
 238 eruption on June 15 1991. Observed plume height (R. Holasek et al., 1996) at different time are
 239 also list in the table.

Eruption duration	4.9 hours	9 hours	10 hours	11.1 hours
Start time	0441	0441	0441	0334
Height at start time	37.5 km	37.5 km	37.5 km	24.5 km
End time	0934	1341	1441	1441
Height at end time	35 km	26.5 km	22.5	22.5 km

243 The new methodology for generating initial ash cloud introduces another new pa-
 244 rameter: elevation threshold. We also carry out sensitivity analysis on this parameter
 245 by varying the elevation threshold from 1500m (the height of the vent) to 25000m. The
 246 simulated ash distributions show obviously visible differences. Such influence is especially
 247 obvious when the elevation threshold is either very large or very small. However, vary-
 248 ing the elevation threshold in the range of [12000, 18000]m generates relatively small dif-
 249 ference in ash transportation simulation results. Figure 5 compares the simulated ash
 250 distribution corresponding to elevation thresholds of 1500m and 15000m. Compared with
 251 ash distribution for threshold of 15000m, an extra long tail appears when using eleva-
 252 tion threshold of 1500m. Adopting smaller elevation thresholds essentially adds more tra-
 253 ckers at lower elevation. As the wind at different elevations are different, these newly added
 254 tracers at lower elevation would transpose to different directions.



255 **Figure 5.** Simulated ash distribution taking initial ash clouds obtained using different el-
 256 evation thresholds (1500m and 15000 m) from output of Plume-SPH. The contours are cor-
 257 responding to ash concentration at 72 hours after eruption. The starting and ending time are
 258 corresponding to 9 hours duration case in Table 2

259 The sensitivity analyses demonstrate that the initial condition for VATD sim-
 260 ulation has the most significant effect on simulated ash distribution while all other input
 261 parameters have either tiny or ignorable influence. The initial ash cloud generated based
 262 on semiempirical expression, which is a function of several parameters, might be signif-
 263 icantly disparate from realistic ash cloud. Such initial condition might greatly compro-
 264 mise the accuracy of VATDs simulation.

265 We do not carry out any investigation with respect to wind field even though it is
 266 another dominant factor in VATD simulation. In the case study, we use global *NOAA/OAR/ESRL6-*
 267 *h, 2.0°* reanalysis wind fields data (Whitaker et al., 2004; Compo et al., 2006, 2011).

268 3 Comparison and Discussion

269 Transportation of volcanic ash resulted from Pinatubo eruption on June 15th 1991
 270 is simulated using two different initial conditions. The initial condition is created in tra-

ditional way according to key global descriptors and semiempirical plume shape expression. The second initial condition is created by the new method proposed in this paper. Simulated ash transportation results are compared against observation.

Table 3. List of eruption condition and material properties for plume simulation

Parameters	Units	Plume
Vent velocity	$m \cdot s^{-1}$	275
Vent gas mass fraction		0.05
Vent Temperature	K	1053
Vent height	m	1500
Mass discharge rate	$kg \cdot s^{-1}$	1.5×10^9
Specific heat of gas at constant volume	$J \cdot kg^{-1} \cdot K^{-1}$	717
Specific heat of air at constant volume	$J \cdot kg^{-1} \cdot K^{-1}$	1340
Specific heat of solid	$J \cdot kg^{-1} \cdot K^{-1}$	1100
Specific heat of gas at constant pressure	$J \cdot kg^{-1} \cdot K^{-1}$	1000
Specific heat of air at constant pressure	$J \cdot kg^{-1} \cdot K^{-1}$	1810
Density of air at vent height	$kg \cdot m^{-3}$	1.104
Pressure at vent height	Pa	84363.4

To create initial condition using the new method described in this paper, the plume raising up process is simulated first by Plume-SPH. The eruption parameters, material properties and atmosphere for the strong plume no wind case in a comparison study on eruptive column models (Costa et al., 2016) are adopted. Eruption conditions and material properties are listed in Table 3. Note that the density of erupted material at the vent and radius of the vent can be computed from the given parameters. The eruption pressure is assumed to be the same as pressure of ambient at the vent and hence is not given in the table. The vertical profiles of atmospheric properties were obtained based on the reanalysis data from ECMWF (European Centre for Medium-Range Weather Forecasts) for the period corresponding to the climactic phase of the Pinatubo eruption. The initial ash cloud is obtained by processing the raw output of Plume-SPH following steps described in Sec. 2.

Another set of initial condition is created based on observed top height (40km) and several other parameters assigned semiempirically (Bursik et al., 2012). These parameters, namely, the global descriptors of volcanic plume, are used as parameters of semiempirical expression to get ash cloud in 3D space. See details in Table 4. The simulation parameters that control VATD simulation are the same for both simulations. As has been shown in sensitivity analyses section, these parameters have less influence on simulation results than initial condition.

3.1 “Plume-SPH + PUFF” and “Semiempirical Initial Cloud + PUFF”

The simulation results using different initial conditions are compared with TOMS images and AVHRR BTD ash cloud map in Fig. 6.

The differences between simulated ash transportation by “Semiempirical initial cloud +PUFF” and “Plume-SPH+PUFF” are obvious. The simulated ash concentration based on initial condition created from Plume-SPH is much closer to observation than that based on semiempirical plume shape expression. Around 23 hours and 31 hours after the beginning of the climactic phase, “Plume-SPH + PUFF” simulation generates ash images that generally close to observational image, especially the location where high concentration ash presents. However, these ash at near west to Pinatubo mountain observed

294 **Table 4.** Parameters used in VATD simulation of the climactic phase of Pinatubo eruption on
 295 June 15 1991. The first six parameters are used by semiempirical expression to create initial ash
 296 cloud. When create initial condition based on Plume-SPH model, these parameters are extracted
 297 from output of Plume-SPH model.

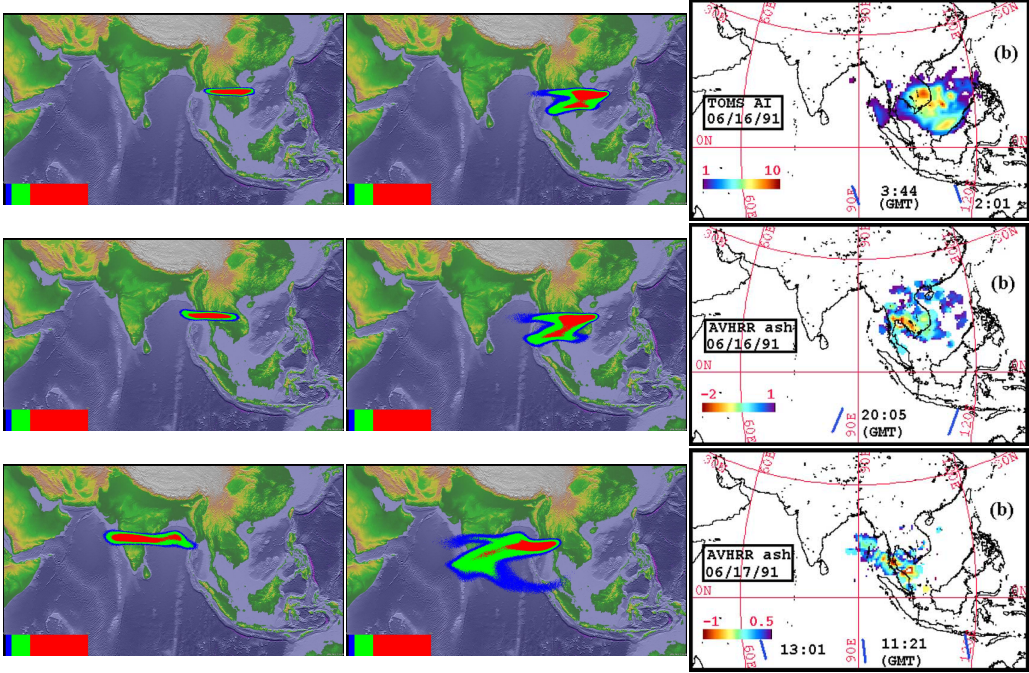
Parameters	Unit	Semiempirical	Plume-SPH
Maximum Height (H_{max})	m	40000	41800
Horizontal Spread (R_{max})	km	103.808	-
Vertical Spread (H_{width})	km	6.662	-
Plume Shape	-	Poisson	-
Total Ash Particles	-	1768500	1768500
Elevation Threshold	m	-	15000
Horizontal Diffusivity	m^2/s	10000	10000
Vertical Diffusivity	m^2/s	10	10
Grain Size Distribution	-	Gaussian	Gaussian
Mean of Grain Size (Radius)	mm	3.5×10^{-2}	3.5×10^{-2}
Standard Deviation of Grain Size	-	1.0	1.0
Start Time	UT	0441	0441
End time	UT	1341	1341
Simulation Duration	hour	72	72

317 in satellite images does not show up in “Plume-SPH + PUFF” simulation results. This
 318 disparity is very possible due to the fact that the Mountain Pinatubo continued erupting
 319 after climactic phase while our simulation only simulates the climactic phase. The
 320 ash released after climactic phase is not accounted in our simulation results. The “Semiem-
 321 pirical initial cloud + PUFF” simulation, however, forecasts an ash distribution faster
 322 and narrower than observation. The location, where the high concentration ash presents,
 323 locates to the far northwest of observed ash. Around 55 hours after the beginning of the
 324 climactic phase, the disparity between observation and simulation becomes more obvi-
 325 ous. Ash distribution of “Semiempirical initial cloud + PUFF” simulation locates far
 326 west to the observed ash. The high concentration area of “Plume-SPH + PUFF” sim-
 327 ulation, even though closer to observation than that of “Semiempirical initial cloud +PUFF”,
 328 is still faster than observation.

329 At the stage of ash transportation simulation, except for the initial condition, both
 330 simulations adopt the same parameters and wind field data. That is to say, the only dif-
 331 ference between these two simulations is the initial condition. Recall the initial condi-
 332 tion has most significant influence on ash transportation simulation. It is very possible
 333 that the big difference between simulation results by “Plume-SPH+PUFF” and “Semiem-
 334 pirical initial cloud +PUFF” is attribute to the initial condition.

335 3.2 Discussion Regarding Maximum Height (H_{max})

336 In this section, we majorly focus on the vertical distribution of ash particles in ini-
 337 tial ash cloud. The majority of volcanic ash particles usually present a lower elevation
 338 than maximum height. For instance, R. Holasek et al. (1996); R. E. Holasek et al. (1996)
 339 reported the maximum Pinatubo plume height as high as around 39km while the cloud
 340 heights were estimated at 20 ~ 25km, Self et al. (1996) report the maximum plume height
 341 could be > 35km and the plume heights are 23 ~ 28km after 15 ~ 16 hours. The neu-
 342 tral buoyant regions of the Pinatubo aerosol estimated by different measurements are:
 343 17 ~ 26km (lidar) by DeFoor et al. (1992), 20 ~ 23km (balloon) by Deshler et al. (1992),
 344 17 ~ 28km (lidar) by Jäger (1992), and 17 ~ 25km (lidar) by Avdyushin et al. (1993).



301 **Figure 6.** Comparison between “Semiempirical initial cloud + PUFF” and “Plume-SPH
 302 + PUFF”. Pictures from left to right are: PUFF simulation based on initial condition created
 303 according to semiempirical plume shape expression, PUFF simulation based on initial condi-
 304 tion generated by Plume-SPH, TOMS or AVHRR image of Pinatubo ash cloud. Ash clouds at
 305 different hours after eruption are on different rows. From top to bottom, the images are corre-
 306 sponding to around 23 hours after eruption (UT 199106160341), 31 hours after eruption (UT
 307 199106161141), 55 hours after eruption (UT 199106171141). The observation data on the first
 308 row are TOMS ash and ice map. The observation data on the second and third row are AVHRR
 309 BTD ash cloud map with atmospheric correction method applied (Guo, Rose, et al., 2004).

345 Based on comparison between simulated cloud with early infrared satellite images of Pinatubo,
 346 Fero et al. (2008) reported that the majority of ash was transported between 16km and
 347 18km. This is physically understandable as particles are concentrated along intrusion
 348 height of umbrella cloud, not near top because the plume top is due to momentum over-
 349 shoot. However, the empirical expressions for the height-MER relation, which are com-
 350 monly adopted to create initial conditions for VATD simulation, tends to place major-
 351 ity of ash particles closer to top if use observed maximum height in the empirical expres-
 352 sions.

353 Here we check two commonly used plume shapes, the Poisson and Suzuki. For Pois-
 354 son plume shape, the vertical height of ash particles are determined according to Eq. (2).

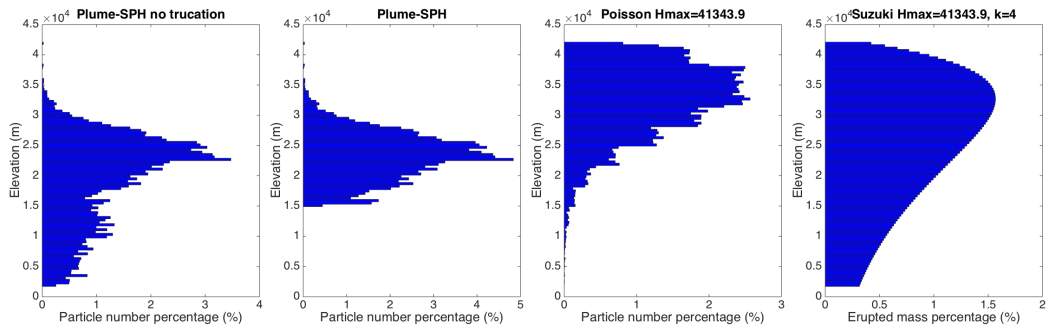
$$H = H_{max} - 0.5H_{width} * P + H_{width}R \quad (2)$$

355 where P is an integral value drawn from a Poisson distribution of unit mean, R is a uni-
 356 formly distributed random number between 0 and 1, H_{max} is the maximum plume height,
 357 H_{width} represents an approximate vertical range over which the ash will be distributed.
 358 For Suzuki plume shape (T. Suzuki et al., 1983), volcano ash mass vertical distribution
 359 is assumed to follow the Suzuki equation (Eq. (3)).

$$Q(z) = Q_m * \frac{k^2(1 - z/H_{max})\exp(k(z/H_{max} - 1))}{H_{max}[1 - (1 + k)\exp(-k)]} \quad (3)$$

360 Where Q_m is the total mass of erupted material, k is shape factor, which is an adjustable
 361 constant that controls ash distribution with height. A low value of k gives a roughly uni-
 362 form distribution of mass with elevation, while high values of k concentrate mass near
 363 the plume top.

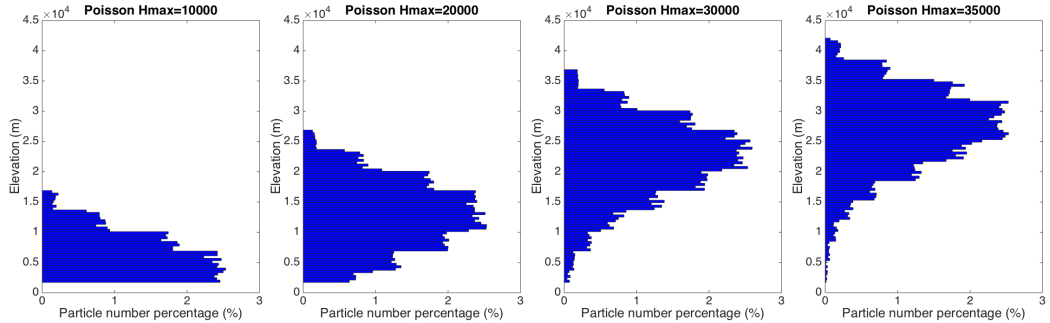
364 Particle distribution (in terms of mass percentage or particle number percentage)
 365 in vertical direction in the initial ash cloud are shown in Fig. 7. In that figure, the ver-
 366 tical particle distribution based on Plume-SPH output is compared with vertical par-
 367 ticle distribution created based on semiempirical shape expressions. Both Poisson and Suzuki
 368 distribution in Fig. 7 take $H_{max} = 40000m$, which is close to reported observation of
 369 maximum height. When adopting Poisson plume shape, the majority of the particles are
 370 between $30km \sim 40km$. Obviously, Poisson distributes majority ash at a much higher
 371 elevation than observations (e.g. Fero et al., 2008). As for Suzuki, the majority of ash
 372 particles also distribute in a range that significantly higher than $25km$. As for initial ash
 373 cloud based on Plume-SPH simulation, the major population of ash particles distribute
 374 between $17km \sim 28km$, which match well with observations. The maximum height is
 375 also consistent with observation. To summarize, using semiempirical plume shape ex-
 376 pression generates unrealistic initial ash cloud even if we use observed plume maximum
 377 height.



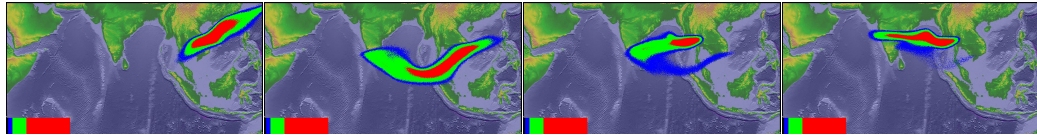
378 **Figure 7.** Particle distribution of initial ash cloud in vertical direction. The picture to the
 379 left is corresponding to initial ash cloud obtained from Plume-SPH output. The second picture
 380 is corresponding to ash distribution truncated by a elevation threshold of $15000m$. The third
 381 picture is for vertical ash distribution based on Poisson distribution with maximum height equals
 382 to $40000m$. Another parameter, the vertical spread, in the expression of Poisson plume shape is
 383 $6662m$. The picture to the right is corresponding to Suzuki distribution with maximum height
 384 equals to $40000m$. Another parameter in Suzuki distribution, the shape factor, is 4. The x axis is
 385 the percentage of particle number for Plume-SPH and Poisson. For Suzuki the x axis is the mass
 386 percentage of erupted material.

387 For Poisson and Suzuki plume shape, vertical distribution of ash particles can't be
 388 lower down without changing the maximum height. To distribute major population of
 389 ash particles at lower elevation, the maximum height has to be reduced to a value smaller
 390 than observed maximum height. Adjusting parameters such as maximum height in the
 391 emperical expression is actually the traditional source term calibration method. A set
 392 of initial ash clouds using different maximum heights based on Poisson plume shape is
 393 shown in Fig. 8). The maximum heights adopted in plume shape expressions are, by no
 394 means, obtained from any plume model or observation. Except for maximum height, all
 395 other parameters for creating initial ash cloud are the same as these in Table 4. The range,
 396 between which major populations of ash particles locate, is lower when using smaller max-
 397 imum heights. These ash clouds created by Poisson distribution with different maximum

398 heights are then used as initial condition in PUFF simulation, whose results are show
 399 in Fig. 9.



400 **Figure 8.** Initial particle distribution in vertical direction based on Poisson plume shape with
 401 different maximum heights. Pictures from left to right are corresponding to maximum height of
 402 10000m, 20000m, 30000m, 35000m. Another parameter, the vertical spread, in the expression of
 403 Poisson plume shape is 6662m for all cases. The x axis is the percentage of particle number. See
 404 Fig. 7 for vertical ash distribution of Plume-SPH output.



405 **Figure 9.** Ash transportation simulated by PUFF using different initial ash cloud created
 406 according to Poisson distribution with different maximum heights. Pictures from left to right are
 407 corresponding to maximum plume heights of 10000m, 20000m, 30000m and 35000m. All images
 408 are for simulated ash transportation around 55 hours after eruption (UT 199106171141). See the
 409 observed cloud image in Fig. 6.

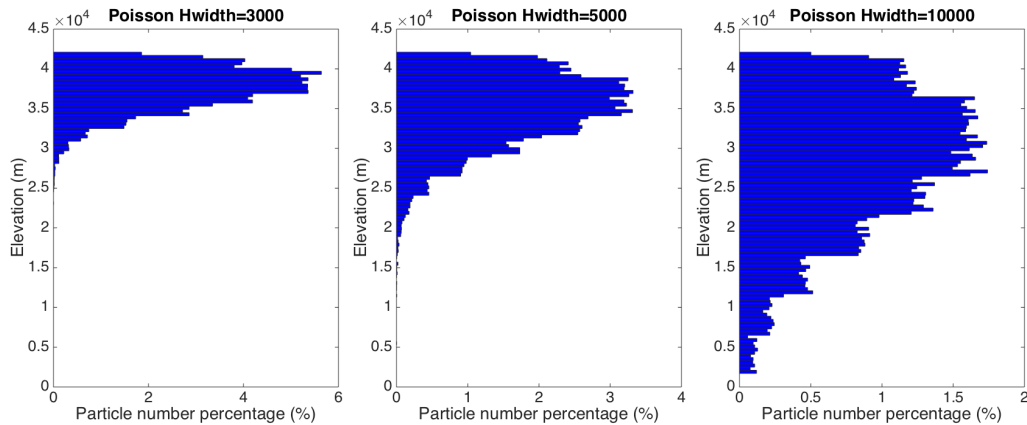
410 Figure 9 shows that the maximum height has significant influence on ash transportation
 411 simulation. When the maximum height is 10000m the high concentration area is
 412 lag behind observation. While the designated maximum height is 35000m, the high con-
 413 centration area is a little bit faster and much narrower than observation. When using
 414 maximum height of 41343.9m, the high concentration area is faster and narrower than
 415 both observation and “Pume-SPH+PUFF” simulation results (see Fig. 6). The sim-
 416 ulated high concentration area is closest to “Pume-SPH+PUFF” simulation results when
 417 assigning a maximum height of 30000m. The front of volcano ash, with lower concen-
 418 tration is faster than observation locating far west to high concentration area. A lower
 419 concentration tailing area also appears in the simulation results while there is no such
 420 tail in observed image. PUFF simulation result based on calibrated maximum height of
 421 30000m shows similar footprint to, even though smaller in terms of covered area than,
 422 those of “Pume-SPH+PUFF” simulation. However, the initial ash cloud created by Pois-
 423 son distribution with maximum height around 20000m generates best match ash distri-
 424 bution with observation. That is to say, a maximum height lower than real maximum
 425 height is required by Poisson plume shape to distribute ash particles at the same eleva-
 426 tion as real ash distribution. This is physically understandable as maximum plume heights
 427 are reached due to overshoot. Our hypothesis regarding the sources of disparity between
 428 “Semiempirical initial cloud +PUFF” simulation and observation is confirmed. Since the

429 initial condition has so dominant effect on VATD simulation, it is very necessary to ex-
 430 plore more accurate and adaptive ways for establishing the initial conditions.

431 3.3 Discussion Regarding Vertical Spread (H_{width})

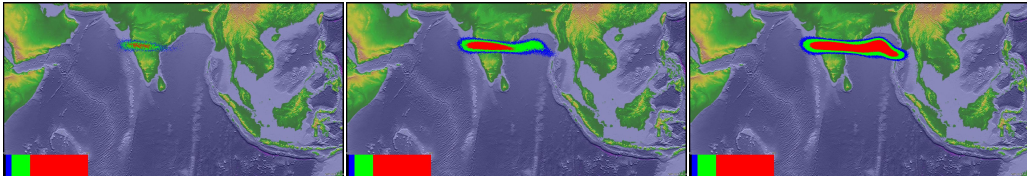
432 In previous section, the maximum height is adjusted to change vertical ash distri-
 433 bution along the source line. This section investigates another parameter in semiempir-
 434 ical poisson expression. We vary the “vertical spread” (H_{width}) in range $3km/ 10km$.
 435 A set of initial ash clouds created according to different “vertical spread” is shown in Fig.
 436 10. Except for “vertical spread”, all other parameters for creating initial ash cloud are
 437 the same as these in Table 4. Width of the range within which major populations of ash
 438 particles locate become narrower when a smaller value for vertical spread is used. But
 439 changing H_{width} has no obvious affect on the height at which majority of ash particles
 440 distribute. These ash clouds based on different vertical spread are then used as initial
 441 condition in PUFF simulation, whose results are show in Fig. 11.

442 Adjusting of the vertical spread can change particle distribution in vertical direc-
 443 tion and not surprisingly affect VATD simulation results. Unluckily, none of these VATD
 444 simulations based on initial ash cloud with vertical spread equals to $3km$, $5km$, and $10km$
 445 get better results than VATD simulation based on initial condition created by a 3D plume
 446 simulation using Plume-SPH (see Fig. 11).



447 **Figure 10.** Vertical particle distribution based on Poisson plume shape with different “ver-
 448 tical spread”. Pictures from left to right are corresponding to vertical spread of $3km$, $5km$ and
 449 $10km$. The maximum height in the expression of Poisson plume shape is $40000m$ for all cases.
 450 The x axis is the percentage of particle number. See Fig. 7 for vertical ash distribution of Plume-
 451 SPH output.

457 The calibrations carried out here are definitely not exhaustive. One might do more
 458 comprehensive calibration throughout the multi-dimensional (two dimensional for Pois-
 459 son distribution) parameter space and get better matched ash transportation results. With
 460 more complicated plume shape expression, one could have more control over plume shape
 461 and might be able to get initial condition that much closer to actual initial ash cloud,
 462 hence obtain more accurate ash transportation prediction. But more complicated plume
 463 shape expression usually leads to higher dimensional parameter space which requires more
 464 effort to do calibration. Even though, the degree of freedom to adjust plume shape is still
 465 limited. The new method for creating initial conditions based on 3D plume simulation
 466 is more adaptive to various cases and obviates semiempirical expressions regarding plume
 467 shape.



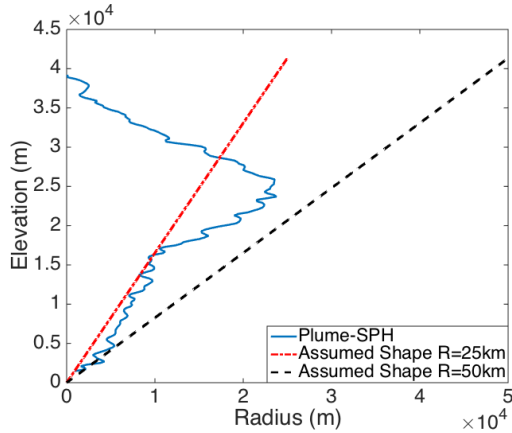
452 **Figure 11.** Ash transportation simulated by PUFF using different initial ash cloud created
 453 with different vertical spread. Pictures from left to right are: PUFF simulation results based on
 454 initial ash clouds with vertical spread equals to 3000mm , 5000mm and 10000m . The images are
 455 corresponding to around 55 hours after eruption (UT 199106171141). See the observed cloud
 456 image in Fig. 6. The simulated ash field does not adequately cover the observed ash field.

468 3.4 Horizontal Ash Distribution

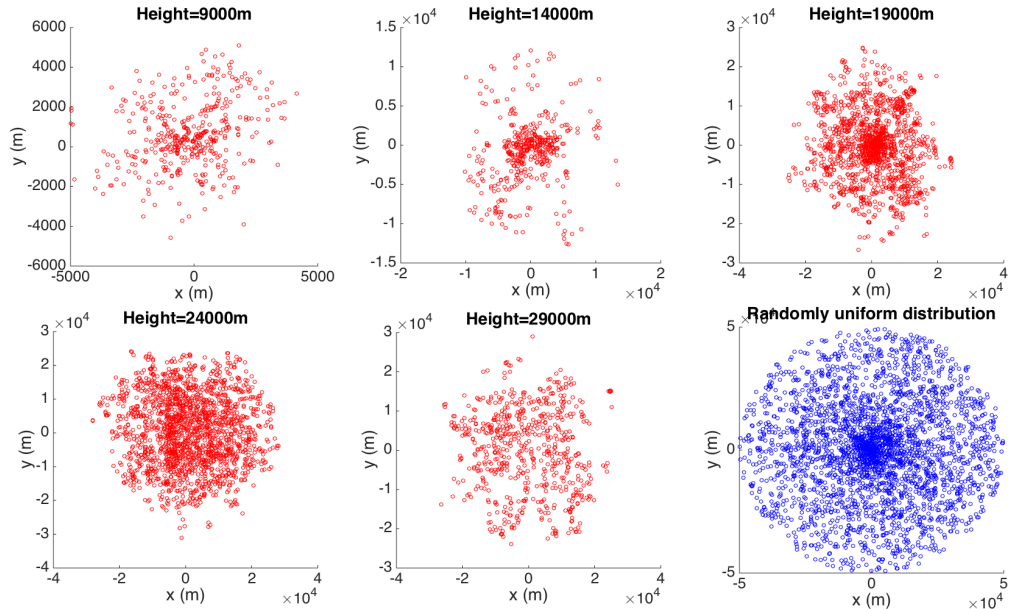
469 The differences between assumed plume particle distribution and actual (or sim-
 470 ulated by 3D plume) model are not only in vertical direction. How cloud horizontal par-
 471 ticle distribution of the initial ash cloud affect ash transportation is investigated in this
 472 section. PUFF uses a uniformly distributed random process to determine the ash par-
 473 ticle location in a circle centered on the volcano site. The maximum radius (at top) is
 474 given as “horizontal spread” in Table 4. The horizontal displacement from a vertical line
 475 above the volcano is a random value within a circle of radius, which equals to “horiz-
 476 onal spread” multiplied by the ratio of the particle height H to maximum H_{max} . So the
 477 net shape of the plume is an inverted cone where particles are located directly over the
 478 volcano at the lowest level and extend out further horizontally with increasing plume height.
 479 As for output of Plume-SPH, an effective radius is determined according to a given thresh-
 480 old of ash concentration following Cerminara, Esposti Ongaro, & Neri (2016). A time
 481 averaging and spatial integration of the dynamic 3D flow fields are conducted to get rid
 482 of significant fluctuations in time and space. Fig. 12 compares radius of initial ash clouds
 483 created by 3D plume simulation and assumed plume shape expression adopted in PUFF.
 484 Obviously, there is no chance for these two radius to be similar. Adjusting the param-
 485 eter “horizontal spread” could not make the assumed plume shape to be similar to ash
 486 cloud created by Plume-SPH. That is to say, merely parameter calibration is not enough
 487 for such situation. It would require higher order semiempirical expression that takes more
 488 parameters.

494 Comparison between cross-sectional views of the initial ash clouds is shown in Fig.
 495 13. The cross-sectional view of assumed plume shape (last figure in Fig. 13) is similar
 496 to cross-sectional view of simulated 3D plume in general sense. However, for simulated
 497 3D plume, the ash particle distribution on cross section varies along with height. It is
 498 hard for semiempirical expressions have such feature. In PUFF, particle distribution on
 499 cross sections is assumed to be the same.

504 Assigning different values to “horizontal spread” has ignorable effect on VATD sim-
 505 ulation results. We use numbers between 50km to 1600km as “horizontal spread” to cre-
 506 ate initial ash cloud for VATD, all of them generate very similar results. Figure ?? shows
 507 two different simulation results based on initial ash cloud with “horizontal spread” equals
 508 to 50km and 600km respectively. No visible differences can be told between them. This
 509 implies that horizontal distribution has less significant influence on VATD simulation re-
 510 sults than vertical distribution.



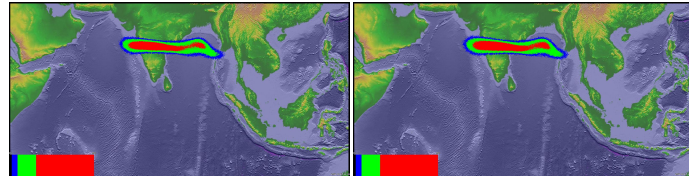
489 **Figure 12.** Comparison between radius of initial ash clouds created by 3D plume model
 490 (Plume-SPH) and assumed initial ash cloud shape in PUFF. The plume shape expression used
 491 in PUFF defines an inverted cone whose actual shape changes when “horizontal spread” takes
 492 different values. $R = 25\text{km}$ is corresponding to “horizontal spread” equals to 50km . $R = 50\text{km}$ is
 493 corresponding to “horizontal spread” equals to 100km



500 **Figure 13.** Horizontal distribution of ash particles (tracers) on a cross section of initial ash
 501 cloud. PUFF assumes randomly uniform distribution of ash particle within a circle, as shown
 502 by red dots in the last figure. All other figures show ash particle distribution of initial ash cloud
 503 created by Plume-SPH at different elevations.

515 4 Conclusion

516 This paper presented, for the first time, VATD simulation using intial condition
 517 created by a 3D plume model while traditional VATD simulation using initial condition
 518 created according to semiempirical plume shape expression. Case study of Pinatubo erup-
 519 tion demonstrates that 3D plume model can create more realistic initial ash cloud and
 520 improve accuracy of ash transportation forecast. In order to explain why we got much



511 **Figure 14.** Ash transportation simulated by PUFF at around 55 hours after eruption (UT
 512 199106171141). Different values for “horizontal spread” are used to create initial ash cloud.
 513 Pictures to the left is corresponding to “horizontal spread” equals to 50kmm. Pictures to the right is
 514 corresponding to “horizontal spread” equals to 600kmm. The observed cloud image is in Fig. 6.

521 closer ash dispersal forecast merely by adopting alternative initial conditions, more in-
 522 vestigations were conducted. Sensitivity analyses illustrate that initial condition has more
 523 significant effects on volcanic ash transportation forecast than most of the other param-
 524 eters. Comparison of vertical ash distribution between 3D plume model, semiempirical
 525 expression and observations reveals that major population of ash particles are at much
 526 lower elevation than maximum height. For the case study of Pinatubo eruption, “well-
 527 matched” simulation results are observed when using maximum height of around 30km,
 528 which is much lower than observed maximum height of 40km. Calibrating of the max-
 529 imum height, vertical spread and horizontal spread shows that ash particle distribution
 530 in vertical direction has more dominant effect on VATD simulation.

531 This new method provides an alternative option for creating initial conditions for
 532 VATD simulation. Except for the disadvantage of high computational cost it helps over-
 533 come several shortcomings of existing methods. As numerical models based on first prin-
 534 ciple, 3D plume models eliminate parameterization and hence user intervention associ-
 535 ated with entrainment coefficients, thereby, improve forecast capacity of ash transpor-
 536 tation simulation. More importantly, no assumption about plume shape is needed in this
 537 new method. The plume shape generated directly by 3D simulation is more adaptive to
 538 various scenarios, thereby, could be more realistic. Contrastingly, semiempirical plume
 539 shape expressions only have several parameters to control the vertical ash particle dis-
 540 tribution of line source or the shape of initial ash cloud, it might have difficulties to gen-
 541 erate initial condition that close to reality for some eruptions. In theory, the method-
 542 ology can be applied to any combination of VATD model and 3D plume model even though
 543 a specific 3D plume model and VATD model is used in this paper.

544 The full range of research issues raised by the numerical forecasting of volcanic clouds
 545 is many and diverse. We described in this paper the effect of initial conditions on nu-
 546 merical forecasts of volcanic ash transportation simulation. Wind field, another impor-
 547 tant factor in volcanic ash transportation simulation is not discussed in the present work.
 548 Some other aspects, such as small scale physical processes, even though plays less roles,
 549 might need to be included by VATDs to improve accuracy for particular eruption event.
 550 In addition, the eruption condition, hence the initial ash clouds, are subject to change
 551 during eruption even during climactic phase of eruption. More realistic, time-dependent,
 552 initial condition for VATDs can be created from 3D plume simulation with time-dependent
 553 eruption conditions.

554 Acknowledgments

555 Support for the Twentieth Century Reanalysis Project dataset is provided by the U.S.
 556 Department of Energy, Office of Science Innovative and Novel Computational Impact
 557 on Theory and Experiment (DOE INCITE) program, and Office of Biological and En-
 558 vironmental Research (BER), and by the National Oceanic and Atmospheric Adminis-
 559 tration Climate Program Office.

560 **References**

- 561 Avdyushin, S., Tulinov, G., Ivanov, M., Kuzmenko, B., Mezhuev, I., Nardi, B., ...
 562 Chanin, M.-L. (1993). 1. spatial and temporal evolution of the optical thick-
 563 ness of the pinatubo aerosol cloud in the northern hemisphere from a network of
 564 ship-borne and stationary lidars. *Geophysical research letters*, 20(18), 1963–1966.
- 565 Bonadonna, C., & Houghton, B. (2005). Total grain-size distribution and volume of
 566 tephra-fall deposits. *Bulletin of Volcanology*, 67(5), 441–456.
- 567 Bursik, M. (2001). Effect of wind on the rise height of volcanic plumes. *Geophys.
 568 Res. Lett.*, 28(18), 3621–3624.
- 569 Bursik, M., Jones, M., Carn, S., Dean, K., Patra, A., Pavolonis, M., ... others
 570 (2012). Estimation and propagation of volcanic source parameter uncertainty in
 571 an ash transport and dispersal model: application to the eyjafjallajokull plume of
 572 14–16 april 2010. *Bulletin of volcanology*, 74(10), 2321–2338.
- 573 Cao, Z., Patra, A., Bursik, M., Pitman, E. B., & Jones, M. (2018). Plume-sph 1.0:
 574 a three-dimensional, dusty-gas volcanic plume model based on smoothed particle
 575 hydrodynamics. *Geoscientific Model Development*, 11(7), 2691–2715.
- 576 Cerminara, M., Esposti Ongaro, T., & Berselli, L. (2016). Ashee-1.0: a compressible,
 577 equilibrium-eulerian model for volcanic ash plumes. *Geoscientific Model Develop-
 578 ment*, 9(2), 697–730.
- 579 Cerminara, M., Esposti Ongaro, T., & Neri, A. (2016). Large eddy simulation of
 580 gas-particle kinematic decoupling and turbulent entrainment in volcanic plumes.
 581 *Journal of Volcanology and Geothermal Research*.
- 582 Compo, G. P., Whitaker, J. S., & Sardeshmukh, P. D. (2006). Feasibility of a 100-
 583 year reanalysis using only surface pressure data. *Bulletin of the American Meteo-
 584 rological Society*, 87(2), 175–190.
- 585 Compo, G. P., Whitaker, J. S., Sardeshmukh, P. D., Matsui, N., Allan, R. J., Yin,
 586 X., ... others (2011). The twentieth century reanalysis project. *Quarterly Journal
 587 of the Royal Meteorological Society*, 137(654), 1–28.
- 588 Costa, A., Suzuki, Y., Cerminara, M., Devenish, B., Esposti Ongaro, T., Herzog, M.,
 589 ... others (2016). Results of the eruptive column model inter-comparison study.
 590 *Journal of Volcanology and Geothermal Research*.
- 591 Daniele, P., Lirer, L., Petrosino, P., Spinelli, N., & Peterson, R. (2009). Applications
 592 of the puff model to forecasts of volcanic clouds dispersal from etna and vesuvio.
 593 *Computers & Geosciences*, 35(5), 1035–1049.
- 594 DeFoor, T. E., Robinson, E., & Ryan, S. (1992). Early lidar observations of the june
 595 1991 pinatubo eruption plume at mauna loa observatory, hawaii. *Geophysical re-
 596 search letters*, 19(2), 187–190.
- 597 Degruyter, W., & Bonadonna, C. (2012). Improving on mass flow rate estimates of
 598 volcanic eruptions. *Geophysical Research Letters*, 39(16).
- 599 de'Michieli Vitturi, M., Neri, A., & Barsotti, S. (2015). Plume-mom 1.0: A new
 600 integral model of volcanic plumes based on the method of moments. *Geoscientific
 601 Model Development*, 8(8), 2447–2463.
- 602 Deshler, T., Hofmann, D., Johnson, B., & Rozier, W. (1992). Balloonborne measure-
 603 ments of the pinatubo aerosol size distribution and volatility at laramie, wyoming
 604 during the summer of 1991. *Geophysical research letters*, 19(2), 199–202.
- 605 Devenish, B. (2013). Using simple plume models to refine the source mass flux
 606 of volcanic eruptions according to atmospheric conditions. *Journal of Volcanology
 607 and Geothermal Research*, 256, 118–127.
- 608 Draxler, R. R., & Hess, G. (1998). An overview of the hysplit_4 modelling system for
 609 trajectories. *Australian meteorological magazine*, 47(4), 295–308.
- 610 D'amours, R. (1998). Modeling the etex plume dispersion with the canadian emer-
 611 gency response model. *Atmospheric Environment*, 32(24), 4335–4341.
- 612 Fero, J., Carey, S. N., & Merrill, J. T. (2008). Simulation of the 1980 eruption

- of mount st. helens using the ash-tracking model puff. *Journal of Volcanology and Geothermal Research*, 175(3), 355–366.
- Fero, J., Carey, S. N., & Merrill, J. T. (2009). Simulating the dispersal of tephra from the 1991 pinatubo eruption: implications for the formation of widespread ash layers. *Journal of Volcanology and Geothermal Research*, 186(1), 120–131.
- Folch, A., Costa, A., & Macedonio, G. (2009). Fall3d: A computational model for transport and deposition of volcanic ash. *Computers & Geosciences*, 35(6), 1334–1342.
- Folch, A., Costa, A., & Macedonio, G. (2016). Fplume-1.0: An integral volcanic plume model accounting for ash aggregation. *Geoscientific Model Development*, 9(1), 431.
- Guo, S., Bluth, G. J., Rose, W. I., Watson, I. M., & Prata, A. (2004). Re-evaluation of so₂ release of the 15 june 1991 pinatubo eruption using ultraviolet and infrared satellite sensors. *Geochemistry, Geophysics, Geosystems*, 5(4).
- Guo, S., Rose, W. I., Bluth, G. J., & Watson, I. M. (2004). Particles in the great pinatubo volcanic cloud of june 1991: The role of ice. *Geochemistry, Geophysics, Geosystems*, 5(5).
- Holasek, R., Self, S., & Woods, A. (1996). Satellite observations and interpretation of the 1991 mount pinatubo eruption plumes. *Journal of Geophysical Research: Solid Earth*, 101(B12), 27635–27655.
- Holasek, R. E., Woods, A. W., & Self, S. (1996). Experiments on gas-ash separation processes in volcanic umbrella plumes. *Journal of volcanology and geothermal research*, 70(3-4), 169–181.
- Jäger, H. (1992). The pinatubo eruption cloud observed by lidar at garmisch-partenkirchen. *Geophysical research letters*, 19(2), 191–194.
- Mastin, L. G. (2007). A user-friendly one-dimensional model for wet volcanic plumes. *Geochemistry, Geophysics, Geosystems*, 8(3).
- Neri, A., Esposti Ongaro, T., Macedonio, G., & Gidaspow, D. (2003). Multiparticle simulation of collapsing volcanic columns and pyroclastic flow. *Journal of Geophysical Research: Solid Earth (1978–2012)*, 108(B4).
- Oberhuber, J. M., Herzog, M., Graf, H.-F., & Schwanke, K. (1998). Volcanic plume simulation on large scales. *Journal of Volcanology and Geothermal Research*, 87(1), 29–53.
- Paladio-Melosantos, M. L. O., Solidum, R. U., Scott, W. E., Quiambao, R. B., Umabal, J. V., Rodolfo, K. S., ... Ruelo, H. B. (1996). Tephra falls of the 1991 eruptions of mount pinatubo. *Fire and mud*, 12000, 12030.
- Pouget, S., Bursik, M., Singla, P., & Singh, T. (2016). Sensitivity analysis of a one-dimensional model of a volcanic plume with particle fallout and collapse behavior. *Journal of Volcanology and Geothermal Research*.
- Schwaiger, H. F., Denlinger, R. P., & Mastin, L. G. (2012). Ash3d: A finite-volume, conservative numerical model for ash transport and tephra deposition. *Journal of Geophysical Research: Solid Earth*, 117(B4).
- Scott, W. E., Hoblitt, R. P., Torres, R. C., Self, S., Martinez, M. M. L., & Nillos, T. (1996). Pyroclastic flows of the june 15, 1991, climactic eruption of mount pinatubo. *Fire and Mud: eruptions and lahars of Mount Pinatubo, Philippines*, 545–570.
- Searcy, C., Dean, K., & Stringer, W. (1998). Puff: A volcanic ash tracking and prediction model. *Journal of Volcanology and Geothermal Research*, 80, 1–16.
- Self, S., Zhao, J.-X., Holasek, R. E., Torres, R. C., & King, A. J. (1996). The atmospheric impact of the 1991 mount pinatubo eruption.
- Stefanescu, E., Patra, A., Bursik, M., Madankan, R., Pouget, S., Jones, M., ... others (2014). Temporal, probabilistic mapping of ash clouds using wind field stochastic variability and uncertain eruption source parameters: Example of the 14 april 2010 eyjafjallajökull eruption. *Journal of Advances in Modeling Earth*

- 667 *Systems*, 6(4), 1173–1184.
- 668 Suzuki, T., et al. (1983). A theoretical model for dispersion of tephra. *Arc volcanism: physics and tectonics*, 95, 113.
- 670 Suzuki, Y., & Koyaguchi, T. (2009). A three-dimensional numerical simulation of
671 spreading umbrella clouds. *Journal of Geophysical Research: Solid Earth (1978–2012)*, 114(B3).
- 673 Suzuki, Y. J., Koyaguchi, T., Ogawa, M., & Hachisu, I. (2005). A numerical study
674 of turbulent mixing in eruption clouds using a three-dimensional fluid dynamics
675 model. *Journal of Geophysical Research: Solid Earth*, 110(B8).
- 676 Tanaka, H. (1991). Development of a prediction scheme for the volcanic ash fall
677 from redoubt volcano. In *First int'l. symp. on volcanic ash and aviation safety*
678 (Vol. 58).
- 679 Walko, R., Tremback, C., & Bell, M. (1995). Hypact: The hybrid particle and con-
680 centration transport model. *User's guide*.
- 681 Whitaker, J. S., Compo, G. P., Wei, X., & Hamill, T. M. (2004). Reanalysis without
682 radiosondes using ensemble data assimilation. *Monthly Weather Review*, 132(5),
683 1190–1200.
- 684 Witham, C., Hort, M., Potts, R., Servranckx, R., Husson, P., & Bonnardot, F.
685 (2007). Comparison of vaac atmospheric dispersion models using the 1 november
686 2004 grimsvötn eruption. *Meteorological Applications*, 14(1), 27–38.
- 687 Woodhouse, M., Hogg, A., Phillips, J., & Sparks, R. (2013). Interaction between vol-
688 canic plumes and wind during the 2010 eyjafjallajökull eruption, iceland. *Journal of Geophysical Research: Solid Earth*, 118(1), 92–109.
- 689 Woods, A. (1988). The fluid dynamics and thermodynamics of eruption columns.
690 *Bulletin of Volcanology*, 50(3), 169–193.
- 691 Zidikheri, M. J., Lucas, C., & Potts, R. J. (2017). Estimation of optimal dispersion
692 model source parameters using satellite detections of volcanic ash. *Journal of Geo-
693 physical Research: Atmospheres*, 122(15), 8207–8232.
- 694